Remote Sensing of Environment xxx (2015) xxx–xxx

Contents lists available at ScienceDirect

Remote Sensing of Environment

journal homepage: www.elsevier.com/locate/rse

Landsat 8 and ICESat-2: Performance and potential synergies for quantifying dryland ecosystem vegetation cover and biomass ☆

Nancy F. Glenn [a,*], Amy Neuenschwander [b], Lee A. Vierling [c], Lucas Spaete [a], Aihua Li [a], Douglas J. Shinneman [d], David S. Pilliod [d], Robert S. Arkle [d], Susan K. McIlroy [d]

[a] Boise Center Aerospace Laboratory, Department of Geosciences, Boise State University, 1910 University Drive, Boise, ID 83725-1535, USA
[b] Geospatial Laser Applications and Measurements, Applied Research Laboratories, University of Texas at Austin, 10000 Burnet Rd, Austin, TX 78758, USA
[c] Department of Natural Resources and Society, University of Idaho, 875 Perimeter Drive MS 1133, Moscow, ID 83844-1133, USA
[d] US Geological Survey Forest and Rangeland Ecosystem Science Center, 970 Lusk Street, Boise, ID 83706, USA

ARTICLE INFO

Article history:
Received 6 May 2015
Received in revised form 4 February 2016
Accepted 17 February 2016
Available online xxxx

Keywords:
OLI
TM
ATLAS
ICESat-2
MABEL
Above-ground biomass
Shrub

ABSTRACT

The Landsat 8 mission provides new opportunities for quantifying the distribution of above-ground carbon at moderate spatial resolution across the globe, and in particular drylands. Furthermore, coupled with structural information from space-based and airborne laser altimetry, Landsat 8 provides powerful capabilities for large-area, long-term studies that quantify temporal and spatial changes in above-ground biomass and cover. With the planned launch of ICESat-2 in 2017 and thus the potential to couple Landsat 8 and ICESat-2 data, we have unprecedented opportunities to address key challenges in drylands, including quantifying fuel loads, habitat quality, biodiversity, carbon cycling, and desertification.

In this study, we explore the strengths of Landsat 8's Operational Land Imager (OLI) in estimating vegetation structure in a dryland ecosystem, and compare these results to Landsat 5's Thematic Mapper (TM). We also demonstrate the potential of OLI when coupled with light detection and ranging (lidar) in estimating vegetation cover and biomass in a dryland ecosystem. The OLI and TM predictions were similarly positive, indicating data from these sensors may be used in tandem for long-term time-series analysis. Results indicate shrub and herbaceous cover are well predicted with multi-temporal OLI data, and a combination of OLI and lidar derivatives improves most of these estimates and reduces uncertainty. For example, significant improvements were made for shrub cover ($R^2 = 0.64$ and 0.78 using OLI only and both OLI and lidar data, respectively). Importantly, a time series of OLI, with some improvement from lidar, provides strong estimates of herbaceous cover (68% of the variance is explained with OLI alone). In contrast, OLI data explain roughly 59% of the variance in total shrub biomass, however approximately 71% of the variance is explained when combined with lidar derivatives.

To estimate the potential synergies of OLI and ICESat-2 we used simulated ICESat-2 photon data to predict vegetation structure. In a shrubland environment with a vegetation mean height of 1 m and mean vegetation cover of 33%, vegetation photons are able to explain nearly 50% of the variance in vegetation height. These results, and those from a comparison site, suggest that a lower detection threshold of ICESat-2 may be in the range of 30% canopy cover and roughly 1 m height in comparable dryland environments and these detection thresholds could be used to combine future ICESat-2 photon data with OLI spectral data for improved vegetation structure. Overall, the synergistic use of Landsat 8 and ICESat-2 may improve estimates of above-ground biomass and carbon storage in drylands that meet these minimum thresholds, increasing our ability to monitor drylands for fuel loading and the potential to sequester carbon.

1. Introduction

Global drylands, which include hyper-arid, arid, semiarid, and dry-subhumid ecosystems, are undergoing rapid population growth and are highly sensitive to climate change (Reynolds et al., 2007). Globally, drylands cover over 40% of the Earth's surface providing ecosystem services to one-third of the world population (MEA, 2005a). These ecosystem services include water and soil-related services such as cultivated croplands and rangelands. Although total biomass and soil organic carbon are not highly concentrated in drylands, their geographic extent results in providing a role in climate regulation through carbon sequestration (MEA, 2005b). Yet drought and population growth, coupled with intensified land use, can result in desertification (Geist &

☆ For submission to *Special Issue of Remote Sensing of Environment on Landsat 8 Science Results.*

* Corresponding author.
E-mail address: nancyglenn@boisestate.edu (N.F. Glenn).

http://dx.doi.org/10.1016/j.rse.2016.02.039
0034-4257/

Lambin, 2004) and cause considerable changes in vegetation (e.g. D'Antonio & Vitousek, 1992) and loss of net primary production and soil carbon (Lal, 2004, Zika & Erb, 2009). Previous studies of global drylands have indicated that maintaining plant biodiversity may help mitigate disturbance in drylands (Maestre et al., 2012). Monitoring vegetation cover and biomass over time and space can assess desertification trends at the global scale, and management practices at the regional or local scale (e.g. Hellden & Tottrup, 2008, Prince, Becker-Reshef, & Rishmawi, 2009).

The long-term data record of Landsat sensors offers opportunities to globally monitor ecosystem and land use change in dryland systems. For example, at the regional level dryland ecosystem studies have used Landsat time-series analyses to assess land cover change (Sonnenschein, Kuemmerle, Udelhoven, Stellmes, & Hostert, 2011), regional woody vegetation cover (Asner, Archer, Hughes, Ansley, & Wessman, 2003), and shifts in land management practices (Stellmes, Udelhoven, Roder, Sonnenschein, & Hill, 2010). Challenges associated with dryland vegetation monitoring using the Landsat spectral bands and spatial scale, including strong soil-vegetation spectral mixing due to the high percent bare ground and inherently sparse vegetation cover, might be improved with Landsat 8's Operational Land Imager (OLI). With a pushbroom configuration, OLI has at least an eight fold increase in signal-to-noise ratio than previous Landsat missions, along with spectrally narrower optical bands, potentially improving detection of vegetation parameters in environments with strong soil and vegetation spectral mixing (Roy et al., 2014). To our knowledge, one study has been published using OLI to assess dryland vegetation structure. In particular, OLI-derived metrics were used to estimate shrub biomass in Tajikistan, resulting in estimates comparable to finer spatial resolution RapidEye imagery (Zandler, Brenning, & Samimi, 2015). A gap also exists in understanding OLI's performance in dryland characterization in comparison to previous Landsat missions, including Thematic Mapper (TM) and Enhanced Thematic Mapper plus (ETM+), such that data from several of these missions can be used together for long-term retrospective analyses.

Several studies have incorporated lidar (light detection and ranging) data with optical data to improve upon spectral and spatial limitations of Landsat TM and ETM+. For example, Garcia, Riano, Chuvieco, Salas, & Danson (2011) mapped fuel types in Mediterranean shrubs and trees and Ji et al. (2012) estimated above ground biomass of trees, shrubs, and herbaceous vegetation types in Alaska. Similar work has been explored extensively to estimate forest attributes including height (Hudak, Lefsky, Cohen, & Berterretche, 2002, Wulder, Han, White, Sweda, & Tsuzuki, 2007, Wulder et al., 2009, Kellndorfer et al., 2010), cover (Chen, Vierling, Rowell, & DeFelice, 2004), productivity, (Lefsky, Turner, Guzy, & Cohen, 2005b), and species composition (Hill & Thomson, 2005), among others. A recent study by Pflugmacher, Cohen, Kennedy, & Yang (2014) used Landsat and lidar to study aboveground biomass change by back projecting attributes using the Landsat record.

A limitation of incorporating lidar with Landsat is that the studies are typically confined to the areal extent of the lidar, and thus often smaller than an individual Landsat scene. Broader areal extents provided by satellite-based laser altimetry are synergistic with Landsat scene sizes. ICESat's Geoscience Laser Altimeter System (GLAS) has been used with optical imagery in forest ecosystems to estimate forest vertical structure and aboveground biomass (Boudreau et al., 2008, Helmer, Lefsky, & Roberts, 2009, Nelson et al., 2009, Simard, Pinto, Fisher, & Baccini, 2011, Lefsky et al., 2005a), degradation and deforestation, (Margono et al., 2012, Goetz, Sun, Baccini, & Beck, 2010), and growth rates (Dolan, Masek, Huang, & Sun, 2009). Although a previous study in a savannah ecosystem successfully used GLAS for vegetation height characteristics in flat terrain (Khalefa et al., 2013), GLAS's broad footprint and vertical resolution generally have limited applicability in dryland systems. As part of the US National Research Council Decadal Survey, ICESat-2's upcoming Advanced Topographic Laser Altimeter System (ATLAS) will use a multi-beam, micropulse laser, based on a NASA IIP (instrument incubator program) project (Degnan, 2002a) and later developed into usable technology for satellite laser ranging, atmospheric investigations and high altitude/space-based land altimetry. The ATLAS instrument will split a single 532 nm laser beam into 3 pairs of beams approximately 3 km apart on the surface at a pulse repetition rate of 10 kHz. Each pair will have a designated strong beam and weak beam based on their relative energy densities which will help detect surfaces of both high and low reflectivity. Based on the average satellite velocity associated with the planned 572 km altitude orbit for ICESat-2 and the repetition rate, the laser footprints on the surface will be displaced approximately 70 cm for each laser shot. Furthermore, each of the 6 laser footprints from ICESat-2 will ideally have a diameter of ~14 m. The beam configuration as proposed for ICESat-2 is beneficial for terrestrial ecosystems studies because it enables a denser spatial sampling than what was achieved with ICESat's GLAS and the footprint size is complementary to the size of a Landsat pixel. To achieve the dense spatial sampling goal of better than 2 km between equatorial ground tracks, ICESat-2 will be off-nadir pointed a maximum of 1.8 degrees from the reference ground track in the mid-latitudes (approximately 60S to 60 N). An additional benefit to the ecosystem community is the nature of the measurement in the along-track direction. Because of the dense along-track spacing (70 cm) of the ICESat-2 laser shots, estimation of canopy height in areas of topographic relief (i.e. slopes > 5 degrees) should be available. Despite the hardware differences between GLAS and ATLAS, the concept of laser ranging for each of the two systems remains the same; the travel time of each detected photon is used to determine a range to the surface which, when combined with satellite attitude and pointing information, can be geolocated into a unique XYZ location on or near the Earth's surface. The number of detected photons per laser shot is a function of outgoing laser energy, detector hardware, surface reflectance, and solar background noise. Multiple photomultiplier tubes (PMT) with independent timing channels can potentially record multiple photoelectron events for each outgoing laser pulse (Degnan, 2002a, Degnan, 2002b). So, given a single laser pulse, photon-counting systems using PMTs typically accumulate many single photon ranges as reflections from surfaces in addition to optical and electrical noise. The presence of noise presents a new challenge to the process of extracting ground and vegetation signal photons from the collected data as there is no distinction between signal and noise within the PMT detections.

In preparation for the ICESat-2 mission, the Multiple Altimeter Beam Experimental Lidar (MABEL) instrument was developed by NASA as a test-bed representation, or demonstrator instrument, for ATLAS. MABEL is a highly sensitive lidar instrument with single photon detection capability, a repetition rate of 5 kHz, low laser pulse energy and produces both 532 nm and 1064 nm wavelengths (McGill, Markus, Scott, & Neumann, 2013). MABEL was designed to provide a realistic 'simulation' of ICESat-2 conditions given the relevant atmospheric propagation distance from a MABEL 20 km flight altitude and similar expectation of signal to noise and detection thresholds. In addition to providing an indication of expected signal response over specific types of terrain and targets, and data volume requirements, the recent availability of MABEL data has also facilitated preliminary development of new surface extraction algorithms for the photon-counting data in preparation for ICESat-2. During 2014, MABEL completed nearly 45 h of flights at a 20 km altitude over selected sites in Alaska and the Arctic Ocean as well as during the transit from California to Fairbanks, AK. During these flights MABEL collected data over a diverse set of surface types, reflectance, and topography and also completed many calibration exercises to ensure the quality of the data. Studies exploring MABEL's data qualities for ground and vegetation characteristics will allow more rapid adoption of ATLAS data products once available. Importantly, the added value of using ATLAS's ground elevation and vegetation height data with OLI's spectral responses should be explored for potential added value to OLI data products.

Please cite this article as: Glenn, N.F., et al., Landsat 8 and ICESat-2: Performance and potential synergies for quantifying dryland ecosystem vegetation cover and biomass, *Remote Sensing of Environment* (2015), http://dx.doi.org/10.1016/j.rse.2016.02.039

The goals of this study are multifold. First, we document OLI's capabilities to quantify vegetation in a shrub-dominated dryland ecosystem by testing the hypothesis that the narrower spectral bands and improved signal-to-noise ratio (SNR) of OLI relative to Landsat TM data will improve finer-level predictions of vegetation characteristics (i.e. shrub and herbaceous vegetation biomass and cover). Second, we explore the additive contribution of integrating OLI and lidar data to improve estimates of vegetation structure, including above-ground biomass in this shrub-dominated dryland site. Third, we explore the potential for ATLAS-estimated MABEL data to contribute to OLI's estimates of vegetation structure, with anticipation that Landsat 8 and ICESat-2 may have synergistic qualities that will advance vegetation and biogeochemical sciences in dryland ecosystems.

2. Study area

To accomplish our study goals, we investigated two semiarid vegetation sites in southwestern Idaho, located in the northern Great Basin in the western U.S. These sites were chosen because of their representative vegetation and soil characteristics that typify dryland systems. Co-located field plots, MABEL, airborne discrete return lidar, OLI, and TM data were readily available for integration and testing (Fig. 1). The first site is the Morley Nelson Snake River Birds of Prey (BoP) National Conservation Area where we investigate OLI's capabilities and compare to TM responses, along with discrete-return lidar contributions (hereafter referred to as lidar), to estimate vegetation cover and biomass. At this site, we also explore the interaction of MABEL photon data with the low-height vegetation and estimate relationships between MABEL photons and vegetation structure. We chose a second site, the Reynolds Creek Experimental Watershed, to further extend the MABEL studies and investigate the utility of photon signals in taller and denser vegetation cover.

The BoP National Conservation Area encompasses over 2400 km^2 of the Snake River Plain ecoregion and is part of the Department of Interior Bureau of Land Management's National Landscape Conservation System. Mean annual temperature is 10.7 °C and mean annual precipitation is 23 cm in the BoP. The area is characterized by relatively flat topography, loess soils, and basalt outcrops. In the last 30 years, the BoP has experienced considerable conversion and fragmentation of its native sagebrush (*Artemisia tridentata*) communities due to climate, fire, land use, and invasive species. Dominant shrubs include Wyoming big sagebrush (*A. tridentata* subsp. *wyomingensis*), rabbitbrush (*Chrysothamnus ericameria*), winterfat (*Krascheninnikovia lanata*), and shadscale (*Atriplex confertifolia*). The open canopy of shrubs is interspersed with native perennial grasses including Sandberg bluegrass (*Poa secunda*), annual invasive grasses such as cheatgrass (*Bromus tectorum*), invasive forbs such as mustards (Brassicaceae family, *Sisymbrium altissimum* among the most common), and biological soil crusts. Over half of the area has burned since 1980. The resulting landscape is a mosaic of plant communities, with compositions spanning a gradient between intact native shrublands, shrublands degraded by non-native plants and wildfire, and grasslands where native plants have been fully replaced by cheatgrass and other invasive annuals. Currently 37% or less of the BoP retains an intact native shrubland community. Recent active management to promote native vegetation and reduce wildfire hazard has been implemented through strategic grazing, mechanical planting of native species, and mowing (USDI BLM 2008).

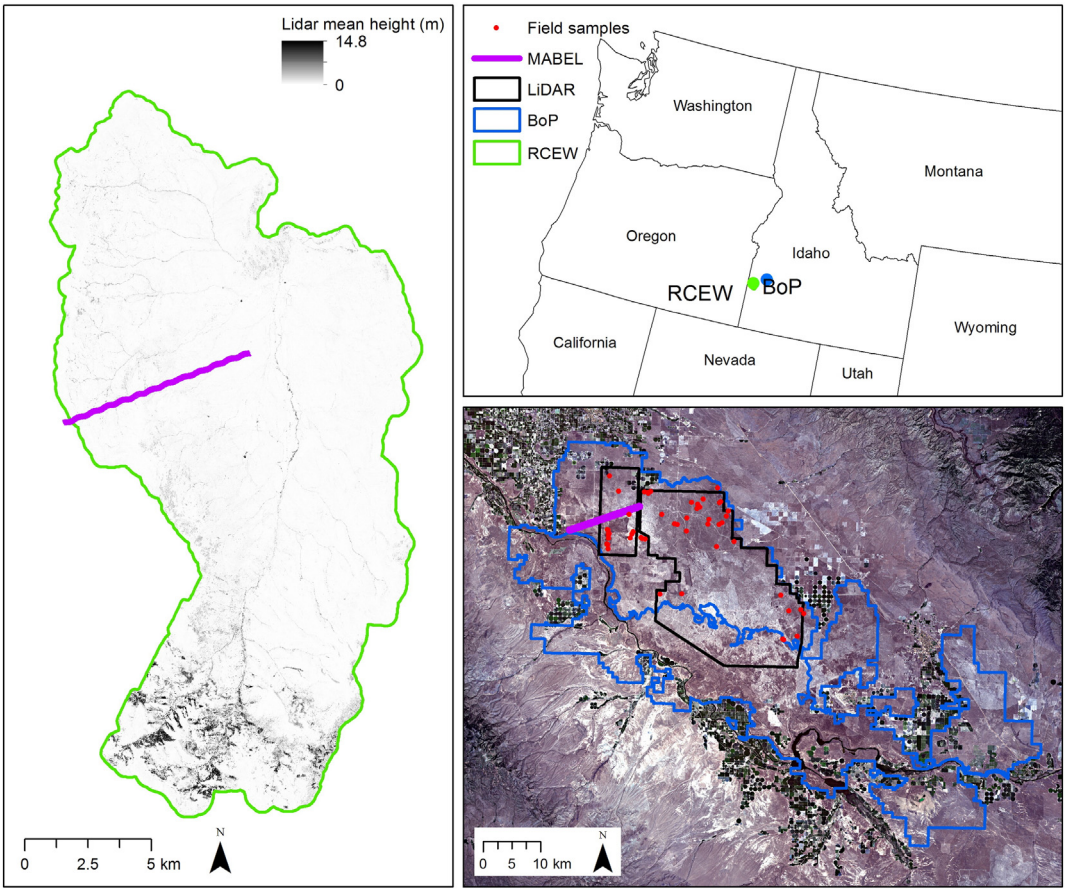

Fig. 1. Reynolds Creek Experimental Watershed (RCEW) (left) and Morley Nelson Snake River Birds of Prey (BoP) National Conservation Area (lower right) study areas, Great Basin, western U.S. Field samples and discrete return lidar data collection sites are shown for the BoP. MABEL data flight locations are shown for both RCEW and BoP. The background RCEW image is lidar-derived mean vegetation height and the background BoP image is an OLI natural-color composite.

Please cite this article as: Glenn, N.F., et al., Landsat 8 and ICESat-2: Performance and potential synergies for quantifying dryland ecosystem vegetation cover and biomass, *Remote Sensing of Environment* (2015), http://dx.doi.org/10.1016/j.rse.2016.02.039

The second study area is located within the 238 km^2 Reynolds Creek Experimental Watershed (RCEW), which is instrumented and monitored by the USDA Agriculture Research Service (ARS). RCEW is approximately 80 km south of Boise, in the Owyhee Mountains. Mean annual temperature below 1500 m and above 1800 m is 7.2 °C and 3.9 °C, respectively. Mean annual precipitation in the watershed is 40 cm. Vegetation varies by elevation, ranging from sagebrush communities in the lower elevation to dryland forest communities dominated with western juniper (*Juniperus occidentalis*), aspen (*Populus tremuloides*), subalpine fir (*Abies lasiocarpa*) and Douglas-fir (*Pseudotsuga menziesii*) at higher elevations. Shrub and grass species dominated the study site where MABEL data were available at RCEW. These shrub communities included low sagebrush (*Artemisia arbuscula*), Wyoming and mountain big sagebrush (*A. tridentata* subsp. *vaseyana*) and bitterbrush (*Purshia tridentata*). Grasses included Bluebunch wheatgrass (*Pseudoroegneria spicata*), Idaho fescue (*Festuca idahoensis*) and cheatgrass.

3. Methods

We used the BoP study site to explore OLI's performance of detecting several canopy cover types, and as a comparison to TM. A secondary goal in the BoP was to test how OLI and lidar integration may improve the vegetation cover and biomass estimates. We also explored relationships between MABEL and cover estimates at BoP and hypothesized that the low height and cover at BoP would not yield a sufficiently strong signal in the MABEL photon dataset. Alternatively, the RCEW study site provided a higher shrub cover and height environment to test the MABEL data and explore potential relationships and associated errors.

At the BoP site, we used an imputation of the OLI and lidar integrated model to provide a spatially-contiguous map of vegetation cover where MABEL data were sampled. MABEL photon data were then compared to the imputed vegetation cover map to identify relationships and associated error between photon signals and vegetation structure. At the RCEW site, we used lidar data only to test MABEL photon sensitivity to vegetation structure.

3.1. Landsat 8 OLI and Landsat 5 TM

A time-series of five OLI images from the 2013 growing season was used from path/row 41/30 covering BoP. The image dates were April 11, June 14, June 30, October 4, and October 20. All other images during 2013 were cloudy. A Landsat 5 TM time series from path/row 41/30 was also used. The 2011 image dates included July 11, July 27, August 12, September 13, and September 29. Images from late spring and early summer had significant cloud cover over the study area. Landsat 5 TM data were not available after late 2011 due to the USGS ceasing routine acquisitions. In addition, Landsat 7 ETM+ data lacked complete coverage over our field samples in 2013. For our comparison, we chose a time delay (between 2011 TM and 2013 OLI data) with a robust sample size (n = 55) in lieu of a similar timeframe (between 2013 ETM+ and 2013 OLI data) that had a lower sample size (n = 22). The OLI and TM images were processed in Google Earth Engine to top-of-atmosphere (TOA) reflectance. The TOA reflectance values were then used to compute a series of vegetation indices at the 30 m pixel scale for each image date (Table 1).

3.2. Airborne discrete return lidar

At the BoP site, airborne discrete return lidar data were collected in 2012 and 2013 using a Leica ALS60. Both discrete return data sets had an average point density of approximately 8 points/m^2. The 2012 data were collected over roughly 650 km^2 of the Orchard Combat Training Center within the BoP and the 2013 data were collected over roughly 90 km^2 (Fig. 1). Vegetation metrics described in Table 2 were computed using height filtered point clouds and represented as 1 m × 1 m cells. These 1 m rasters were then averaged to provide estimates across 30 m cell sizes (i.e. average based on 900 1-m rasters were used to provide one estimate for each 30 m cell to match the OLI pixel size).

Discrete return lidar data were collected in 2007 for the RCEW with a Leica ALS50 and a point density of approximately 4 points/m^2. Vegetation metrics were computed across 3 m × 3 m cells using height filtered point clouds (Glenn et al., 2011). The metrics of the 3 m rasters were then averaged to 30 m cell sizes (i.e. average based on 100 3-m rasters for each 30 m cell). The lidar metrics used at RCEW included maximum vegetation height, mean of the maximum vegetation height, and vegetation cover as estimated from the 100 3-m rasters for each 30 m cell. The vegetation cover was estimated using the same method as Veg_cov in Table 2, and then the mean value was used across the 30 m cell size.

Table 1
Spectral metrics from Landsat 8 OLI used at the BoP.

Metric	Description
Simple Vegetation Index (SVI)	$\frac{NIR}{Red}$
Normalized Difference Vegetation Index (NDVI)	$\frac{NIR-Red}{NIR+Red}$
Soil Adjusted Vegetation Index (SAVI)	$\frac{(NIR-Red)}{NIR+Red+L}(1+L)$ L = 0.25
Modified Soil Adjusted Vegetation Index (MSAVI2)	$\frac{(2NIR+1-\sqrt{(2NIR+1)^2-8(NIR-Red)})}{2}$
Moisture Stress Index (MSI)	$\frac{SWIR}{NIR}$
Moisture Stress Index 2 (MSI2)	$\frac{SWIR2}{NIR}$
Normalized Difference Water Index (NDWI)	$\frac{NIR-SWIR}{NIR+SWIR}$
Normalized Difference Water Index 2 (NDWI2)	$\frac{NIR-SWIR2}{NIR+SWIR2}$

3.3. Mabel

The MABEL instrument was flown over the two study sites July 11, 2014 at a 20 km operating altitude and the data were processed to Level2b by the ICESat-2 Project office at NASA Goddard Space Flight Center. A transect of approximately 7.5 km and 13 km was sampled across RCEW and BoP, respectively. The data were processed using noise filtering and surface finding algorithms developed by the ICESat-2 Science Definition Team (SDT). Contrary to commercial discrete return systems, ATLAS and MABEL are photon counting systems characterized by low signal to noise rates. Solar background noise, in particular, is a significant challenge in the analysis of photon-counting laser data as there is no way to distinguish the photons reflected by a lidar specific wavelength (i.e. signal photons) from those photons returned from the atmosphere or scattered from adjacent targets (i.e.

Table 2
Discrete return lidar metrics used at the BoP. The height in the description includes the heights of all vegetation returns.

Metric	Description
Hmin	Minimum height
Hmax	Maximum height
Hrange	Difference between maximum and minimum heights
Hmean	Average height
HMAD	Median absolute deviation from median height
HAAD	Mean absolute deviation from mean height
Hvar	Variance of height
Hstd	Standard deviation of height
Hskew	Skewness of height
Hkurt	Kurtosis of height
HIQR	Interquartile range (IQR) of height
HCV	Coefficient of variation of height
H5-H95	5th, 10th, 25th, 50th, 75th, 90th, and 95th percentiles of heights
Hcrr	Canopy relief ratio: $(H_{mean} - H_{min})/(H_{max} - H_{min})$
Htext	Texture of height: Standard deviation (height > ground threshold and height < crown threshold)
Veg_cov	Percent ratio of vegetation returns and total returns
Veg_density	Percent ratio of vegetation returns and ground returns

Please cite this article as: Glenn, N.F., et al., Landsat 8 and ICESat-2: Performance and potential synergies for quantifying dryland ecosystem vegetation cover and biomass, *Remote Sensing of Environment* (2015), http://dx.doi.org/10.1016/j.rse.2016.02.039

noise photons); all are collected by the lidar receiver. Solar background noise rates are a combination of the solar zenith angle and the scene reflectance, which is a combination of both the atmosphere and surface. As such, effective filtering techniques must be developed to estimate and filter out background noise. Without this process, the result is prolonged processing time and inaccurate surface estimations. In the ICESat-2 SDT algorithm signal photons can be isolated from noise photons based on an adaptive nearest neighbor search.

For the terrestrial ecosystem community, the ability to detect both the canopy surface and the underlying topography is a critical task. Accurate determination of local, regional and global canopy heights is a primary contributor to many science investigations such as aboveground biomass assessments or carbon monitoring. Although many algorithms exist for extracting canopy heights and terrain from more traditional lidar remote sensing technology, new approaches are required for the photon counting technology. In this study, once the signal photons were identified, they were separated into ground and canopy photons using an iterative filtering method to estimate a ground surface. Photons lying within +/− 1 m of the estimated ground surface were subsequently labeled as ground photons. Photons lying above the ground threshold and were clustered in nature were designated as canopy photons and assigned a height based on the difference of the estimated ground surface and the canopy photon elevation. Photons 5 m above the surface were considered noise and removed from the analysis. The canopy photons were then assigned a vegetation height. This process was performed for each of the eight MABEL near infrared (NIR) channels (e.g. Channels 43–50). Channel 50 was not available for the RCEW dataset due to data errors. The NIR channels were used in this analysis as they have a higher signal to noise ratio and are a closer representation of the expected number of reflected photons that ICESat-2 will return (compared to the green MABEL channels).

Variation in the ground track of the MABEL platform resulted in differing lengths of transects across the 30 m OLI pixels. Therefore, all MABEL photon counts used in the analysis were normalized over the segment (e.g. length) of the MABEL flight across a 30-m pixel. If the line segment length was less than 30 m, the data were discarded from analysis. The MABEL metrics were developed from these normalized photon counts and their respective classifications (e.g. ground and canopy) (Table 3). Metrics were computed on the statistics of the photon heights within each segment length, resulting in standard deviation, skewness, and kurtosis of the canopy and all (canopy and ground) photons (Table 3).

3.4. Field data

At BoP, field plots were established in 2012 and 2013 and consisted of fifty-five 60 m × 60 m plots with nine 1-m^2 quadrats within each plot. The field data extended beyond the MABEL flight line but were located within the lidar boundaries (Fig. 1). An average from the 9 quadrats was used to estimate the vegetation parameters for each plot. Cover was estimated for shrubs, grasses and other herbaceous plants (herbaceous hereafter) in each quadrat using a grid-point intercept analysis of photographs taken at nadir (see Pilliod & Arkle, 2013). Biomass was estimated for all vegetation in the quadrats using oven-dried weights of destructively sampled vegetation classes. We used the following cover and biomass field measurements to relate to the remote sensing data: sagebrush cover, shrub (sagebrush and other shrub species such as rabbitbrush) cover, herbaceous cover, shrub (sagebrush and other shrub species) biomass, herbaceous biomass, and total (shrub and herbaceous) biomass. Field cover estimates indicate that mean fractional shrub and herbaceous cover were roughly 13% and 35%, respectively (Table 4).

3.5. BoP analyses

A random forests analysis (Breiman, 2001) at the BoP was performed with the remote sensing metrics to understand the accuracy and error in predicting the field measurements of vegetation structure. The intent was also to identify the relative contributions of OLI, TM, and lidar. The RF analysis was performed using 1) OLI-only, 2) TM-only, 3) lidar-only, and 4) a combination of OLI and lidar metrics with the field measurements. Sagebrush cover, shrub cover, herbaceous cover, herbaceous biomass, shrub biomass, and total biomass were predicted. The RF analysis was performed using The Salford Predictive Modeler Software Suite (Salford Systems, San Diego CA). Each run used 1000 trees and the number of variables considered at each node was rounded to the closest integer of the square root of the total number of variables considered for each run. Variables were removed from each run based on two relative importance score criteria: 1) a relative importance score less than 10 and 2) if no variables had a relative importance score of less than 10, the lowest scoring variable was removed. Models were considered final when the removal of the lowest scoring variable had a major impact on the overall model fit.

The random forests models using the combined OLI and lidar metrics were then imputed across 30 m pixels using the score function in Salford Systems (San Diego, CA). The score function uses a nearest neighbor lookup approach similar to imputation in R (Crookston & Finley, 2008). The imputation was performed in order to provide a spatially-continuous map to compare to MABEL photons across the locations of the flights. Both OLI and lidar were used for the imputation because the combined metrics provided the lowest error for predicting vegetation structure (discussed below).

MABEL metrics were compared to the BoP imputed vegetation cover and biomass across 30 m cell sizes. We used a random forests analysis for this comparison and to identify potential MABEL metrics that were important variables. MABEL metrics were also compared using random forests to discrete return lidar-derived vegetation height (maximum and mean of the maximum) and vegetation cover (Table 2) at 30 m cell sizes.

3.6. RCEW analyses

Similar to BoP, we compared discrete return lidar-derived vegetation height (maximum and mean of the maximum) and vegetation cover to MABEL metrics across 30 m cell sizes. This comparison was performed using random forests and multiple linear regression. The latter was used as an alternative to the random forests score analysis in order to explore relationships with scatterplots.

Table 3
MABEL metrics used at BoP and RCEW.

Metric
All photon counts normalized by length
Ground photon counts normalized by length
Canopy photon counts normalized by length
Standard deviation of canopy heights
Standard deviation of all photon heights
Kurtosis of canopy height photons
Kurtosis of all photons
Skewness of canopy height photons
Skewness of all photons

Table 4
Statistics of vegetation cover and biomass based on field data (n = 55). Cover is in % and biomass is in grams/m^2.

	Minimum	Maximum	Mean	Standard deviation
Sagebrush cover	0.00	48.06	10.14	13.95
Total shrub cover	0.00	48.06	12.87	14.14
Herbaceous cover	0.00	97.29	37.14	25.37
Herbaceous biomass	31.13	485.23	143.32	82.17
Total shrub biomass	0.00	954.39	208.38	252.40
Total biomass	36.83	1116.83	351.64	279.15

Please cite this article as: Glenn, N.F., et al., Landsat 8 and ICESat-2: Performance and potential synergies for quantifying dryland ecosystem vegetation cover and biomass, *Remote Sensing of Environment* (2015), http://dx.doi.org/10.1016/j.rse.2016.02.039

4. Results

4.1. OLI, TM, lidar, OLI + lidar

Based on the random forest analyses, the use of OLI variables alone explained between 62 and 68% of the variance associated with cover estimates at BoP (Table 5). At least three OLI variables, including a combination of spectral data from two to three OLI acquisition dates, provided the highest explanation of variance for each cover type (sagebrush, shrub, and herbaceous cover). The MSAVI2 and SVI were consistently identified as variables of importance for all cover estimates. The models had a lower explanatory power for shrub and total biomass (e.g. approximate $R^2 = 0.58$) and used MSAVI2, SVI, and NDVI from multiple OLI acquisition dates. In comparison to shrub and total biomass, herbaceous biomass was more poorly explained with OLI data ($R^2 = 0.53$). The predictive power and estimated errors of TM-based indices were similar to the OLI-based indices. Sagebrush cover and shrub biomass were strongly predicted by TM ($R^2 = 0.73$ and $R^2 = 0.64$, respectively) and the RMSE was 1% and 11 g/m^2 lower than the OLI predictions, respectively. Other differences between OLI and TM occurred in predicting shrub ($R^2 = 0.64$ and 0.60, respectively) and herbaceous cover ($R^2 = 0.68$ and 0.54, respectively) and herbaceous biomass ($R^2 = 0.53$ and 0.29, respectively). The MSAVI2 and NDWI2 were used in most of the TM predictions with the exception of shrub and herbaceous cover and herbaceous cover and total biomass, respectively; while the MSI2 was used in all TM predictions except herbaceous biomass. However, the SVI and NDVI were not common predictors in the TM data as compared to the OLI predictions.

When discrete return lidar data were used to create similar predictions, the sagebrush and shrub cover models explained a higher percentage of variance than the OLI models, while the herbaceous cover and biomass were poorly predicted (Table 5). The discrete return lidar metrics of vegetation cover and derivatives of vegetation height were the strongest predictors. Herbaceous cover was poorly predicted with lidar with less than 10% of the variance explained. Using both the OLI and lidar data together increased the model predictions in all cover and biomass types, ranging from R^2 of 0.65 (herbaceous biomass) to R^2 of 0.83 (sagebrush cover) (Table 5). Combining lidar and OLI data also decreased the errors associated with the predictions over using spectral data alone. For example, an approximate 2–3% decrease in prediction error was found for all cover estimates when OLI and discrete return lidar were used together instead of OLI alone. Likewise, biomass error was reduced by 7 to 27 g/m^2 by using both OLI and lidar variables as predictors. As a comparison, when TM data were used with lidar, sagebrush cover estimates increased to R^2 of 0.90 (RMSE of 4.4%; data not shown) and shrub biomass estimates increased to R^2 of 0.74 (RMSE of 127 g/m^2; data not shown). The OLI and lidar random forests models were then imputed across the area covered by the MABEL flights for the MABEL analysis.

4.2. Mabel

The capacity of MABEL to predict vegetation structure was tested at both the BoP and RCEW sites. Random forests was used to explore interactions between predictor and target variables. At the BoP site, there was little to no relationship found between MABEL photon metrics and imputed vegetation biomass and cover. The strongest relationships were in the prediction of shrub cover and vegetation height, with R^2 values ranging from 0.12 to 0.18. For example, we found that imputed shrub cover was best modeled using MABEL metrics of canopy photon counts normalized by length, skewness and kurtosis of canopy photon heights, and standard deviation and kurtosis of all photon heights ($R^2 = 0.12$; RMSE = 11%). In comparison, the mean of the maximum height derived directly from discrete return lidar was best modeled using MABEL metrics of photon counts normalized by length and kurtosis of canopy photon heights ($R^2 = 0.18$; RMSE = 0.06 m). Both of these relationships were found using the MABEL Channel 43; however similar relationships were found in Channel 50.

We found a stronger relationship between discrete return lidar and MABEL datasets at RCEW using random forests. In particular, we found that MABEL canopy photon counts normalized by length and standard deviation of all photon heights from Channel 43 explained roughly 49% (RMSE = 0.34 m) of the variance of the mean of the maximum vegetation height from lidar. Reasonably strong predictions were also made using Channel 49, explaining 35% (RMSE = 0.33 m) of the variance of the mean of the maximum vegetation height using MABEL canopy photon counts normalized by length and all photon counts normalized by length. MABEL canopy photon counts normalized by length and standard deviation of all photon heights from Channel 43 explained roughly 25% (RMSE = 16.2%) of the variance of the mean vegetation cover from lidar. While Channels 43 and 49 are both NIR channels, they are spaced on average 40 m apart. This offset, along with normalizing the photon counts across the 30 m pixels, results in different ground areas sampled and thus the likely cause in variation in explanatory power between channels.

Based on the variables identified in random forests, we used the canopy photon count normalized by length and standard deviation of all photon heights from Channel 43 to develop a multiple linear regression model to predict the lidar mean of the maximum height (Fig. 2). This model had a $R^2 = 0.493$ (Adjusted $R^2 = 0.489$; p-value < 0.001)

Table 5
Random forests results for OLI, TM, discrete return lidar, and combined OLI and lidar at BoP. RMSE is in units of % for cover predictions and grams/m^2 for biomass predictions. The OLI and TM variables are labeled by Julian date and metric from Table 1. The lidar variables are labeled by metric from Table 2. N = 55.

	OLI			TM			Lidar			OLI + lidar		
	R^2	RMSE	Variables	R^2	RMSE	Variables	R^2	RMSE	Variables	R^2	RMSE	Variables
Sagebrush cover	0.62	8.47	L8_165_MSAVI2, L8_165_NDVI, L8_165_SVI, L8_293_MSAVI2	0.73	7.18	L5_208_NDVI, L5_256_MSAVI2, L5_272_MSI2, L5_272_NDWI2	0.74	7.00	Veg_cov	0.83	5.63	L8_165_SVI, Veg_cov
Shrub cover	0.64	8.40	L8_181_SVI, L8_277_SVI, L8_293_MSAVI2	0.60	8.85	L5_224_MSI, L5_272_MSI2, L5_272_NDWI2	0.75	6.90	Hstd, Veg_cov	0.78	6.51	HAAD, H90, L8_101_MSI2, Veg_cov
Herbaceous cover	0.68	14.03	L8_181_MSI2, L8_181_NDWI2, L8_277_SVI	0.54	16.74	L5_208_MSI2, L5_224_MSI, L5_272_MSI2	0.08	23.00	HCV, Hkurt, Hskew	0.73	12.76	L8_181_MSI2, Veg_cov
Herbaceous biomass	0.53	55.97	L8_181_MSAVI2, L8_181_NDWI2, L8_181_SAVI	0.29	68.72	L5_256_MSAVI2, L5_256_NDWI2, L5_272_MSAVI2	0.42	63.00	H10, Hcrr	0.65	48.39	H10, L8_181_MSAVI2
Shrub biomass	0.59	160.93	L8_165_NDVI, L8_165_SAVI, L8_277_SVI, L8_293_MSAVI2	0.64	149.84	L5_192_SAVI, L5_256_MSAVI2, L5_272_MSI2, L5_272_NDWI2	0.56	165.00	H90, Veg_cov	0.71	133.61	H90, L8_293_MSAVI2, L8_277_SVI
Total biomass	0.58	179.97	L8_165_NDVI, L8_277_SVI, L8_293_MSAVI2	0.57	181.95	L5_256_MSAVI2, L5_272_MSI2	0.58	178.94	Hcrr, H90, Veg_cov	0.66	157.08	H90, Oct20_MSI2, Veg_cov

Please cite this article as: Glenn, N.F., et al., Landsat 8 and ICESat-2: Performance and potential synergies for quantifying dryland ecosystem vegetation cover and biomass, *Remote Sensing of Environment* (2015), http://dx.doi.org/10.1016/j.rse.2016.02.039

(RMSE = 0.29 m), similar and as expected to the random forests regression. However, the explained variance in mean height jumped to 63% when one large outlier (a MABEL predicted mean height of 3.46 m) was kept in the analysis (data not shown). Likewise we used the Channel 43 MABEL canopy photon count normalized by length and standard deviation of all photon heights to model the mean vegetation cover of lidar across 30 m, resulting in a $R^2 = 0.244$ (Adjusted $R^2 = 0.236$; p-value <0.001) and RMSE of 16.4% (Fig. 3).

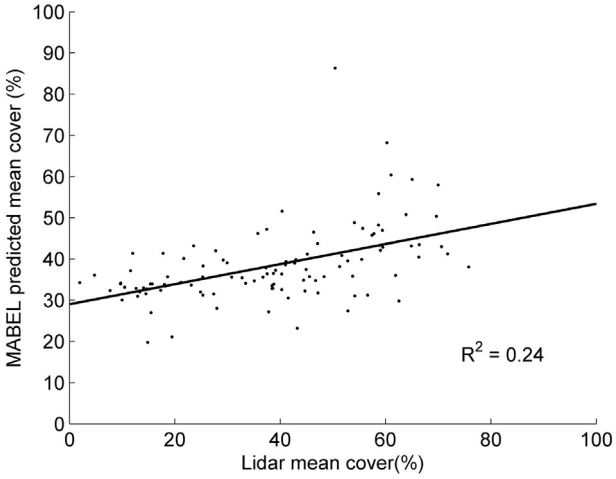

Fig. 3. Multiple linear regression of MABEL canopy photon count normalized by length and standard deviation of all photon heights from Channel 43 to predict mean cover of lidar across 30 m.

5. Discussion

5.1. OLI and TM vegetation cover and biomass comparison

OLI-based prediction of dryland vegetation characteristics performed quite strongly, with both cover and biomass predictions performing on par (or better) with using discrete return lidar data-based prediction alone (Table 5). The coefficient of determination (R^2) for OLI-based vegetation cover prediction was at least 0.62 for all cover types, and with RMSE values between 8.5 and 14%. Biomass estimates all exhibited an R^2 of at least 0.53. Of notable interest is that in all cases, the top OLI-based model to describe vegetation cover fractions and biomass included vegetation indices calculated from multiple acquisition dates. This finding is in agreement with similar results by (Shoshany & Svoray, 2002), who mapped cover of different plant functional types using Landsat TM images acquired across three distinct time periods in a similar short-stature Mediterranean shrubland and dwarf-shrubland ecosystem. Shoshany and Svoray (2002) concluded that differential phenological transitions allowed vegetation from multiple functional groups to be unmixed from each other and from the background soil. This suggests that changing phenological conditions among the vegetation functional groups (shrubs, forbs, and grasses) in the current study may have allowed for sub-pixel discrimination of vegetation cover types relative to the unchanging soil background. The MSAVI2 and SVI were used as predictors in all cover and biomass estimations with the exception of herbaceous cover and herbaceous biomass, respectively.

TM-based predictions performed comparably with OLI for determining vegetation characteristics of all metrics examined in this study, with the exception of the herbaceous classes. The TM-based coefficient of variation of herbaceous biomass (R^2 of 0.29 compared to 0.53 for OLI), as well as the lower capability of TM in explaining variance in herbaceous cover, are likely a result of the two year time gap between field/OLI data and the TM imagery. Herbaceous growth is variable from year to year dependent upon climate, whereas shrub growth (especially for sagebrush) is less pronounced. The result that TM modestly outperformed OLI in explaining variance in sagebrush cover and shrub biomass is difficult to explain, though the seasonal timing of the images of TM relative to OLI may have contributed. The TM images ranged from July to end of September; whereas the OLI images ranged from April to the end of October. As a result, OLI data may have been more influenced by the larger range in image solar zenith angle. Interestingly, many of the multi-date predictors in both OLI and TM were dominated by MSAVI2 but the TM-based predictions relied more heavily on MSI2 and NDWI2, whereas OLI-based predictions often included SVI. However, even in cases where similar indices were employed, a true cross-comparison to understand the reasons for the relative strengths of OLI and TM performance is difficult. For example OLI's NIR band has a narrower bandwidth than TM, and the shift towards longer wavelengths (0.85–0.88 μm for OLI compared to 0.76–0.90 μm of TM) will result in differences in the vegetation indices we used in this study, including the SVI and MSAVI2. Likewise, the OLI SWIR2 band ranges from 2.11–2.29 μm in comparison to TM's SWIR2 ranging from 2.08–2.35 μm (the SWIR2 band is used in the MSI2 and NDWI2 indices). Despite these differences, the fact that TM and OLI performed similarly for predicting most of the vegetation characteristics in this study bodes well for comparing new OLI-based estimates to retrospective analyses using TM data.

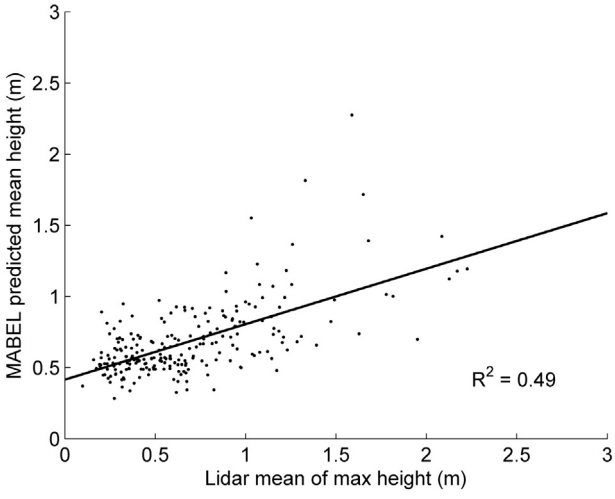

Fig. 2. Multiple linear regression of MABEL canopy photon count normalized by length and standard deviation of all photon heights from Channel 43 to predict the mean of the maximum vegetation height of lidar across 30 m.

5.2. OLI- and discrete return lidar-based vegetation cover and biomass prediction

Cover predictions based on discrete return lidar alone outperformed OLI-only predictions for both sagebrush and shrub cover, exhibiting slightly higher R^2 values and lower RMSE values (Table 5). However, lidar-only based prediction of herbaceous cover was inferior to that predicted by the OLI-only model. When combining both OLI and lidar metrics for vegetation cover prediction, the R^2 and RMSE of the combined model were better than or equal to when either OLI or lidar metrics were used in isolation. Of particular note was the ability for the combined model to predict sagebrush shrub cover, which was predicted with an R^2 of 0.83 and RMSE of only 5.6%. This compares favorably with previous work that used terrestrial laser scanning (TLS) (Vierling, Xu, Eitel, & Oldow, 2012) and hyperspectral and lidar (Mitchell, Shrestha, Spaete, & Glenn, 2015) to estimate sagebrush cover in similar ecosystems. Vierling et al. (2012) found that they could estimate sagebrush cover with an R^2 of 0.51 and an RMSE of 7.0% by using TLS with a point density of hundreds of lidar returns m^{-2}. Mitchell et al. (2015) estimated cover using hyperspectral and discrete return lidar with

58% of the variance explained and RMSE = 7.4%. Their estimates are from sites with an elevation and precipitation gradient resulting in a range of shrub cover and heights, and mixed communities, whereas our BoP site is relatively small in scale and homogeneous. Our results from OLI and lidar need to be tested across similar gradients to determine if prediction strength and accuracy would decrease accordingly. Overall, the improvements of using a combined lidar + OLI model for cover estimation of shrubs highlights the advantage of using structural and spectral data for this functional group of vegetation.

Accurate prediction of vegetation biomass in short-stature ecosystems, even when combining passive and active remote sensing data, is challenging. Because area-wide biomass prediction relates to overall vegetation volume, it is important to be able to characterize both the density (i.e. the 2-D cover) and the height of the vegetation. In forested ecosystems, although biomass prediction using passive optical sensors nearly always results in a significantly higher relative error than when using lidar sensors, using a fusion of these two data types typically results in more accurate forest biomass models by ~10% (Zolkos, Goetz, & Dubayah, 2013).

In the case of low-stature ecosystems such as those investigated here, however, there is a very high potential for passive + lidar data fusion to provide additional predictive power for biomass. This is due to the often observed phenomenon that airborne lidar typically underestimates the true height of vegetation that exhibits a discontinuous or sparse canopy top, such as the case with many shrub (Streutker & Glenn, 2006) and conifer tree species. It is not uncommon for airborne discrete return lidar to underestimate shrub canopy height by +/− 0.30 m (Glenn et al., 2011, Mitchell et al., 2011). Because this underestimation is a significant proportion of the total canopy height of most shrubs at the BoP study area, we expected that the OLI-based metrics would improve remotely sensed shrub biomass predictions. Indeed, this was the case in our study, as the R^2 increased from 0.56 and 0.59 when using lidar- or OLI-based metrics in isolation, respectively, to 0.71 in the combined OLI-lidar model. Similarly, the shrub biomass RMSE decreased from 161 to 165 g/m^2 to 133 g/m^2 under the combined model. In comparison, a study using very high density TLS to predict biomass of similarly small shrubs in arctic tundra within small (0.64 m^2) field plots resulted in an RMSE of 117–119 g (Greaves et al., 2015).

5.3. Relationships with MABEL data and implications for spaceborne lidar assessment of drylands

As an orbiting sensor, the prospect of utilizing ICESat-2 data to provide useful information for measuring and monitoring the structure of global terrestrial ecosystems is tantalizing. Dryland ecosystems present a particularly steep challenge to utilizing ICESat-2 data due to their short stature and sparse cover. Indeed, MABEL data were of limited utility in the relatively short-stature BoP study site, with metrics describing at best only 12% of the variance in shrub cover and 18% of the variance in vegetation height.

However, at the RCEW site characterized by taller and a higher density of shrubs, models using MABEL-derived metrics described 49% of the variance in the mean maximum height (RMSE = 0.34 m). The MABEL-derived metrics performed more poorly with estimating the mean vegetation cover at RCEW (25% of variance explained with a RMSE = 16%). The fact that MABEL-derived metrics showed marked improvement in deriving height metrics at the RCEW site may indicate that this site has vegetation tall enough to overcome the noise floor of current ATLAS/MABEL algorithms. The improvement may also be due to the larger range of vegetation heights present within RCEW. The vegetation "noise floor" is defined by signal photons being segregated into those that occur within +/− 1 m of the predicted ground elevation (ground), and those signal photons that occur above the 1 m buffer (canopy). As a result, this study may reveal the functional lower limit to vegetation height prediction using MABEL, and may indicate the lower limit of the ATLAS sensor to be launched aboard ICESat-2. This finding is consistent with recent work showing that simulated ATLAS returns at the taiga-tundra ecotone of Siberia could not resolve above-ground biomass as fine as 10 kg ha^{-1} (Montesano et al., 2015). Although the taiga-tundra ecotone has many important vegetation structural and functional differences from our current study site, the relatively sparse shrubs and dwarf trees that grow along this ecotone do have some commonalities with the system studied here.

The mean vegetation cover and height where the MABEL flights were collected at RCEW was 33% and 0.64 m (height range of roughly 0 to 5 m), respectively. These estimates were made with lidar collected roughly 7 years before the MABEL data and estimated across 3 m pixels. Applying an error bound to underestimated heights (+/− 0.30 m; Mitchell et al., 2011) indicates that mean heights are near 1 m in this region. While vegetation heights and cover likely increased over the past 7 years, these values provide a lower limit of the sensitivity of MABEL photons in dryland communities. In contrast, for the BoP the 30 m imputation estimated mean shrub cover was 8%, the lidar-derived 1 m vegetation cover was lower than 5% and the maximum vegetation heights ranged from 0 to 1.3 m with a mean value of 0.07 m. Applying a +/− 0.30 m error height bound indicates mean vegetation heights are less than 0.40 m. These results demonstrate the dominance of grasses in the MABEL flight area of the BoP. Thus, from both the BoP and RCEW sites, we conclude that lower limits of the MABEL canopy photon detection is at minimum 30% vegetation cover and 1 m vegetation height.

5.4. Impact of results to land management in dryland ecosystems

Deriving more accurate estimates of both plant cover and biomass across large landscapes in dryland ecosystems may be critical to a suite of resource management and conservation objectives. This is particularly true in landscapes such as the northern Great Basin (where our study sites are located), much of which is rapidly transitioning from native shrub-steppe to nonnative, annual-grassland communities (Bradley, 2010). This conversion is occurring in large part due to changes in the historical fire regimes, as cheatgrass and other nonnative herbaceous species promote more frequent fire and quickly establish and dominate after fire (Balch, Bradley, D'Antonio, & Gomez-Dans, 2013, Brooks et al., 2004). This "annual grass-fire regime" prevents reestablishment of native shrubs and bunchgrasses, most of which are not adapted to short fire-return intervals and don't compete well with invasive annual plant species. The consequences of this conversion include loss of biodiversity (e.g., Anderson & Inouye, 2001, Ostoja & Schupp, 2009), changes in above-ground and below-ground carbon pools (e.g., Rau et al., 2011), changes in soil water availability (e.g., Prater, Obrist, Arnone, & DeLucia, 2006), and altered fine fuel loadings that result in highly dynamic fire regimes (D'Antonio & Vitousek, 1992).

Although the required level of accuracy for estimates of vegetation characteristics depends largely on the intended application, recent research developments and trends in resource management data requirements point to ever increasing demands for greater levels of accuracy. For example, local and landscape scale estimates of sagebrush height and shrub cover are used to determine highly specific habitat requirements for sagebrush-dependent species, including the imperiled greater sage grouse (Stiver et al., 2015). Because field vegetation monitoring protocols are often based on discontinuous line transect field monitoring methods, one strong benefit of our approach is the fact that our results contribute to making spatially contiguous maps for use in management. Since the lidar data improved Landsat-based estimates, it is possible that this broad-scale structural information may lend further improvement to regional- and continental-scale vegetation products (such as LANDFIRE; see sagebrush example in Homer, Aldridge, Meyer, and Schell (2012)). In another example, predictions for wildfire danger and fire behavior typically rely on accurate information for fuel loadings by class (e.g., herbaceous versus woody fuels) as

Please cite this article as: Glenn, N.F., et al., Landsat 8 and ICESat-2: Performance and potential synergies for quantifying dryland ecosystem vegetation cover and biomass, *Remote Sensing of Environment* (2015), http://dx.doi.org/10.1016/j.rse.2016.02.039

well as the cover and continuity of fuel-beds and their related moisture content, factors that affect rate of fire spread, fire-line intensity, and flame length (Anderson, 1982, Jolly, 2007). In the Great Basin, native shrublands continue to shift from relatively discontinuous shrub-bunchgrass cover with variable biomass distribution, to more continuous, non-native, herbaceous fuelbeds that lose fuel moisture quickly. More accurate estimates of highly variable vegetation cover and biomass can contribute to the development of custom fuel models that contain specific fuel loading and moisture estimates, and are used in fire behavior models to help determine appropriate fire suppression response (e.g., Parresol, Scott, Andreu, Prichard, & Kurth, 2012). Deriving more accurate estimates of such fuel characteristics (beyond that contained in commonly used fuel models) may also be critical to obtain accurate estimates of greenhouse gas and other emissions from wildfire (Weise & Wright, 2014). In a final example, spatially contiguous maps of vegetation type and cover are currently being used in the northern Great Basin to identify areas of restoration for species of concern in preparation for potential siting of utilities. Land managers are increasingly asking for improved estimates of vegetation characteristics, as the restoration funding is tied to the level of vegetation health as assessed by vegetation type, cover, and biomass.

The relative performance of MABEL-based metrics in deriving vegetation characteristics at our two study sites indicates that future work to combine MABEL and/or ATLAS data with Landsat 8 OLI data is warranted and may result in unique products for dryland management. Because ATLAS is designed as a profiling lidar collecting along-track measurements using three pairs of lasers, it is likely that its utility in detecting useful vegetation cover and biomass parameters will increase as vegetation density increases from the relatively sparse level found at the RCEW site up to some maximum density yet to be determined (i.e. where the density of the vegetation obscures lidar ground-finding such that retrieving reliable vegetation height information becomes difficult). OLI's time-series spectral data are likely to extend ATLAS's capacity in dryland systems. As a result, future studies to examine synergies between MABEL/ATLAS and OLI data across a more continuous range of vegetation cover and height are likely to reveal thresholds where these two datasets can offer synergistic benefits. For example, because grasslands are experiencing woody encroachment by shrubs (and shrublands are experiencing encroachment by tree species) worldwide, understanding the height and cover thresholds at which these encroaching woody plants can be detected using ATLAS may provide new insights to how combined passive/active remote sensing modeling approaches can quantify woody encroachment dynamics. Similarly, quantifying the replacement of native plant communities (that often have heterogeneous height and cover characteristics) by contiguous stands of non-native species (such as homogeneous canopies of cheatgrass, in the Western United States) may be improved using the combined modeling approaches between passive and active remote sensing data demonstrated here and in an increasingly broader array of work (e.g., Zolkos et al., 2013) worldwide.

Acknowledgements

This project was supported under NASA Terrestrial Ecology award number NNX14AD81G. MABEL data were collected from the ICESat-2 Science Definition Team (SDT) and Early Adopter programs. Special thanks to Tom Neumann. Funding for vegetation data at BoP was provided by the Joint Fire Science Program (Project ID: 11-1-2-30) and the U.S. Geological Survey Forest and Rangeland Ecosystem Science Center. Any use of trade, product, or firm names is for descriptive purposes only and does not imply endorsement by the U.S. Government.

References

Anderson, H.E. (1982). *Aids to determining fuel models for estimating fire behavior.* Ogden, UT: USDA Intermountain Forest and Range Experiment Station.

Anderson, J.E., & Inouye, R.S. (2001). Landscape-scale changes in plant species abundance and biodiversity of a sagebrush steppe over 45 years. *Ecological Monographs*, *71*(4), 531–556.

Asner, G. P., Archer, S., Hughes, R. F., Ansley, R. J. and Wessman, C. A. (2003) 'Net changes in regional woody vegetation cover and carbon storage in Texas Drylands, 1937–1999', Global Change Biology, 9(3), pp. 316–335.

Balch, J.K., Bradley, B.A., D'Antonio, C.M., & Gomez-Dans, J. (2013). Introduced annual grass increases regional fire activity across the arid western USA (1980-2009). *Global Change Biology*, *19*(1), 173–183.

Boudreau, J., Nelson, R.F., Margolis, H.A., Beaudoin, A., Guindon, L., & Kimes, D.S. (2008). Regional aboveground forest biomass using airborne and spaceborne LiDAR in Quebec. *Remote Sensing of Environment*, *112*(10), 3876–3890.

Bradley, B.A. (2010). Assessing ecosystem threats from global and regional change: Hierarchical modeling of risk to sagebrush ecosystems from climate change, land use and invasive species in Nevada, USA. *Ecography*, *33*(1), 198–208.

Breiman, L. (2001). Random forests. *Machine Learning*, *45*(1), 5–32.

Brooks, M.L., D'Antonio, C.M., Richardson, D.M., Grace, J.B., Keeley, J.E., DiTomaso, J.M., ... Pyke, D. (2004). Effects of invasive alien plants on fire regimes. *Bioscience*, *54*(7), 677–688.

Chen, X.X., Vierling, L., Rowell, E., & DeFelice, T. (2004). Using lidar and effective LAI data to evaluate IKONOS and Landsat 7 ETM + vegetation cover estimates in a ponderosa pine forest. *Remote Sensing of Environment*, *91*(1), 14–26.

Crookston, N.L., & Finley, A.O. (2008). yaImpute: An R package for kNN imputation. *Journal of Statistical Software*, *23*(10).

D'Antonio, C.M., & Vitousek, P.M. (1992). Biological invasions by exotic grasses, the grass/fire cycle, and global change. *Annual Review of Ecology and Systematics*, *23*, 63–87.

Degnan, J.J. (2002a). A conceptual design for a spaceborne 3D imaging Lidar. *NASA GSFC, Greenbelt, MD, AIAA paper 2002-0936.*

Degnan, J.J. (2002b). Photon-counting multikilohertz microlaser altimeters for airborne and spaceborne topographic measurements. *Journal of Geodynamics*, *34*(3–4), 503–549.

Dolan, K., Masek, J.G., Huang, C.Q., & Sun, G.Q. (2009). Regional forest growth rates measured by combining ICESat GLAS and Landsat data. *Journal of Geophysical Research-Biogeosciences*, *114*.

Garcia, M., Riano, D., Chuvieco, E., Salas, J., & Danson, F.M. (2011). Multispectral and LiDAR data fusion for fuel type mapping using Support Vector Machine and decision rules. *Remote Sensing of Environment*, *115*(6), 1369–1379.

Geist, H.J., & Lambin, E.F. (2004). Dynamic causal patterns of desertification. *Bioscience*, *54*(9), 817–829.

Glenn, N.F., Spaete, L.P., Sankey, T.T., Derryberry, D.R., Hardegree, S.P., & Mitchell, J.J. (2011). Errors in LiDAR-derived shrub height and crown area on sloped terrain. *Journal of Arid Environments*, *75*(4), 377–382.

Goetz, S.J., Sun, M., Baccini, A., & Beck, P.S.A. (2010). Synergistic use of spaceborne lidar and optical imagery for assessing forest disturbance: An Alaska case study. *Journal of Geophysical Research-Biogeosciences*, *115*.

Greaves, H. E., Vierling, L. A., Eitel, J. U. H., Boelman, N. T., Magney, T. S., Prager, C. M. and Griffin, K. L. (2015) 'Estimating aboveground biomass and leaf area of low-stature Arctic shrubs with terrestrial LiDAR', Remote Sensing of Environment, 164(0), pp. 26–35.

Hellden, U., & Tottrup, C. (2008). Regional desertification: A global synthesis. *Global and Planetary Change*, *64*(3–4), 169–176.

Helmer, E.H., Lefsky, M.A., & Roberts, D.A. (2009). Biomass accumulation rates of Amazonian secondary forest and biomass of old-growth forests from Landsat time series and the Geoscience Laser Altimeter System. *Journal of Applied Remote Sensing*, *3*, 31.

Hill, R.A., & Thomson, A.G. (2005). Mapping woodland species composition and structure using airborne spectral and LiDAR data. *International Journal of Remote Sensing*, *26*(17), 3763–3779.

Homer, C.G., Aldridge, C.L., Meyer, D.K., & Schell, S.J. (2012). Multi-scale remote sensing sagebrush characterization with regression trees over Wyoming, USA: Laying a foundation for monitoring. *International Journal of Applied Earth Observation and Geoinformation*, *14*(1), 233–244.

Hudak, A.T., Lefsky, M.A., Cohen, W.B., & Berterretche, M. (2002). Integration of lidar and Landsat ETM plus data for estimating and mapping forest canopy height. *Remote Sensing of Environment*, *82*(2–3), 397–416.

Ji, L., Wylie, B.K., Nossov, D.R., Peterson, B., Waldrop, M.P., McFarland, J.W., ... Hollingsworth, T.N. (2012). Estimating aboveground biomass in interior Alaska with Landsat data and field measurements. *International Journal of Applied Earth Observation and Geoinformation*, *18*, 451–461.

Jolly, W.M. (2007). Sensitivity of a surface fire spread model and associated fire behaviour fuel models to changes in live fuel moisture. *International Journal of Wildland Fire*, *16*(4), 503–509.

Kellndorfer, J.M., Walker, W.S., LaPoint, E., Kirsch, K., Bishop, J., & Fiske, G. (2010). Statistical fusion of lidar, InSAR, and optical remote sensing data for forest stand height characterization: A regional-scale method based on LVIS, SRTM, Landsat ETM plus, and ancillary data sets. *Journal of Geophysical Research-Biogeosciences*, *115*.

Khalefa, E., Smit, I.P.J., Nickless, A., Archibald, S., Comber, A., & Balzter, H. (2013). Retrieval of savanna vegetation canopy height from ICESat-GLAS spaceborne LiDAR with terrain correction. *IEEE Geoscience and Remote Sensing Letters*, *10*(6), 1439–1443.

Lal, R. (2004). Carbon sequestration in dryland ecosystems. *Environmental Management*, *33*(4), 528–544.

Lefsky, M.A., Harding, D.J., Keller, M., Cohen, W.B., Carabajal, C.C., Espirito-Santo, F.D., ... de Oliveira, R. (2005a). Estimates of forest canopy height and aboveground biomass using ICESat. *Geophysical Research Letters*, *32*(22), 4.

Lefsky, M.A., Turner, D.P., Guzy, M., & Cohen, W.B. (2005b). Combining lidar estimates of aboveground biomass and Landsat estimates of stand age for spatially extensive validation of modeled forest productivity. *Remote Sensing of Environment*, *95*(4), 549–558.

Please cite this article as: Glenn, N.F., et al., Landsat 8 and ICESat-2: Performance and potential synergies for quantifying dryland ecosystem vegetation cover and biomass, *Remote Sensing of Environment* (2015), http://dx.doi.org/10.1016/j.rse.2016.02.039

Maestre, F.T., Quero, J.L., Gotelli, N.J., Escudero, A., Ochoa, V., Delgado-Baquerizo, M., ... Zaady, E. (2012). Plant species richness and ecosystem multifunctionality in global drylands. *Science*, *335*(6065), 214–218.

Margono, B.A., Turubanova, S., Zhuravleva, I., Potapov, P., Tyukavina, A., Baccini, A., ... Hansen, M.C. (2012). Mapping and monitoring deforestation and forest degradation in Sumatra (Indonesia) using Landsat time series data sets from 1990 to 2010. *Environmental Research Letters*, *7*(3), 16.

McGill, M., Markus, T., Scott, V.S., & Neumann, T. (2013). The multiple altimeter beam experimental Lidar (MABEL): An airborne simulator for the ICESat-2 mission. *Journal of Atmospheric and Oceanic Technology*, *30*(2), 345–352.

MEA (2005a). *Current state & trends assessment: Dryland systems*. World Resources Institute, Washington, DC: Millennium Ecosystem Assessment.

MEA (2005b). *Ecosystems and human well-being: Desertification synthesis*. Washington, DC: Millennium Ecosystem Assessment: World Resources Institute.

Mitchell, J.J., Glenn, N.F., Sankey, T.T., Derryberry, D.R., Anderson, M.O., & Hruska, R.C. (2011). Small-footprint lidar estimations of sagebrush canopy characteristics. *Photogrammetric Engineering and Remote Sensing*, *77*(5), 521–530.

Mitchell, J.J., Shrestha, R., Spaete, L.P., & Glenn, N.F. (2015). Combining airborne hyperspectral and LiDAR data across local sites for upscaling shrubland structural information: Lessons for HyspIRI. *Remote Sensing of Environment*, *167*, 98–110.

Montesano, P.M., Rosette, J., Sun, G., North, P., Nelson, R.F., Dubayah, R.O., Ranson, K. J., & Kharuk, V. (2015). The uncertainty of biomass estimates from modeled ICESat-2 returns across a boreal forest gradient. *Remote Sensing of Environment*, *158*, 95–109.

Nelson, R., Boudreau, J., Gregoire, T.G., Margolis, H., Naesset, E., Gobakken, T., & Stahl, G. (2009). Estimating Quebec provincial forest resources using ICESat/GLAS. *Canadian Journal of Forest Research-Revue Canadienne De Recherche Forestiere*, *39*(4), 862–881.

Ostoja, S.M., & Schupp, E.W. (2009). Conversion of sagebrush shrublands to exotic annual grasslands negatively impacts small mammal communities. *Diversity and Distributions*, *15*(5), 863–870.

Parresol, B.R., Scott, J.H., Andreu, A., Prichard, S., & Kurth, L. (2012). Developing custom fire behavior fuel models from ecologically complex fuel structures for upper Atlantic Coastal Plain forests. *Forest Ecology and Management*, *273*, 50–57.

Pflugmacher, D., Cohen, W.B., Kennedy, R.E., & Yang, Z.Q. (2014). Using Landsat-derived disturbance and recovery history and lidar to map forest biomass dynamics. *Remote Sensing of Environment*, *151*, 124–137.

Pilliod, D.S., & Arkle, R.S. (2013). Performance of quantitative vegetation sampling methods across gradients of cover in Great Basin Plant communities. *Rangeland Ecology & Management*, *66*(6), 634–647.

Prater, M.R., Obrist, D., Arnone, J.A., & DeLucia, E.H. (2006). Net carbon exchange and evapotranspiration in postfire and intact sagebrush communities in the Great Basin. *Oecologia*, *146*(4), 595–607.

Prince, S.D., Becker-Reshef, I., & Rishmawi, K. (2009). Detection and mapping of long-term land degradation using local net production scaling: Application to Zimbabwe. *Remote Sensing of Environment*, *113*(5), 1046–1057.

Rau, B.M., Johnson, D.W., Blank, R.R., Lucchesi, A., Caldwell, T.G., & Schupp, E.W. (2011). Transition from sagebrush steppe to annual grass (*Bromus tectorum*): Influence on belowground carbon and nitrogen. *Rangeland Ecology & Management*, *64*(2), 139–147.

Reynolds, J.F., Stafford Smith, D.M., Lambin, E.F., Turner, B.L., Mortimore, M., Batterbury, S.P.J., ... Walker, B. (2007). Global desertification: Building a science for dryland development. *Science*, *316*(5826), 847–851.

Roy, D.P., Wulder, M.A., Loveland, T.R., Woodcock, C.E., Allen, R.G., Anderson, M.C., ... Zhu, Z. (2014). Landsat-8: Science and product vision for terrestrial global change research. *Remote Sensing of Environment*, *145*, 154–172.

Shoshany, M., & Svoray, T. (2002). Multidate adaptive unmixing and its application to analysis of ecosystem transitions along a climatic gradient. *Remote Sensing of Environment*, *82*(1), 5–20.

Simard, M., Pinto, N., Fisher, J.B., & Baccini, A. (2011). Mapping forest canopy height globally with spaceborne lidar. *Journal of Geophysical Research-Biogeosciences*, *116*, 12.

Sonnenschein, R., Kuemmerle, T., Udelhoven, T., Stellmes, M., & Hostert, P. (2011). Differences in Landsat-based trend analyses in drylands due to the choice of vegetation estimate. *Remote Sensing of Environment*, *115*(6), 1408–1420.

Stellmes, M., Udelhoven, T., Roder, A., Sonnenschein, R., & Hill, J. (2010). Dryland observation at local and regional scale - Comparison of Landsat TM/ETM plus and NOAA AVHRR time series. *Remote Sensing of Environment*, *114*(10), 2111–2125.

Stiver, S.J., Rinkes, E.T., Naugle, D.E., Makela, P.D., Nance, D.A., & Karl, J.W. (2015). *Sage-Grouse Habitat Assessment Framework: A multiscale assessment tool*. Denver, Colorado: Bureau of Land Management and Western Association of Fish and Wildlife Agencies.

Streutker, D., & Glenn, N. (2006). LiDAR measurement of sagebrush steppe vegetation heights. *Remote Sensing of Environment*, *102*(1–2), 135–145.

Vierling, L.A., Xu, Y.Y., Eitel, J.U.H., & Oldow, J.S. (2012). Shrub characterization using terrestrial laser scanning and implications for airborne LiDAR assessment. *Canadian Journal of Remote Sensing*, *38*(6), 709–722.

Weise, D.R., & Wright, C.S. (2014). Wild land fire emissions, carbon and climate: Characterizing wildland fuels. *Forest Ecology and Management*, *317*, 26–40.

Wulder, M.A., Han, T., White, J.C., Sweda, T., & Tsuzuki, H. (2007). Integrating profiling LIDAR with Landsat data for regional boreal forest canopy attribute estimation and change characterization. *Remote Sensing of Environment*, *110*(1), 123–137.

Wulder, M.A., White, J.C., Alvarez, F., Han, T., Rogan, J., & Hawkes, B. (2009). Characterizing boreal forest wildfire with multi-temporal Landsat and LIDAR data. *Remote Sensing of Environment*, *113*(7), 1540–1555.

Zandler, H., Brenning, A., & Samimi, C. (2015). Quantifying dwarf shrub biomass in an arid environment: comparing empirical methods in a high dimensional setting. *Remote Sensing of Environment*, *158*, 140–155.

Zika, M., & Erb, K. -H. (2009). The global loss of net primary production resulting from human-induced soil degradation in drylands. *Ecological Economics*, *69*(2), 310–318.

Zolkos, S.G., Goetz, S.J., & Dubayah, R. (2013). A meta-analysis of terrestrial aboveground biomass estimation using lidar remote sensing. *Remote Sensing of Environment*, *128*, 289–298.

Please cite this article as: Glenn, N.F., et al., Landsat 8 and ICESat-2: Performance and potential synergies for quantifying dryland ecosystem vegetation cover and biomass, *Remote Sensing of Environment* (2015), http://dx.doi.org/10.1016/j.rse.2016.02.039